

Nuclei Segmentation using a Level Set Active Contour Method and Spatial Fuzzy C-means Clustering

Ravali Edulapuram¹, R. Joe Stanley¹, Rodney Long², Sameer Antani², George Thoma²,
Rosemary Zuna³, William V. Stoecker⁴ and Jason Hagerty^{1,4}

¹Missouri University of Science and Technology, Department of Electrical and Computer Engineering, Rolla, MO, U.S.A.

²Lister Hill Center for Biomedical Communications, National Library of Medicine,
National Institutes of Health, Bethesda, MD, U.S.A.

³University of Oklahoma, University of Oklahoma Health Sciences Center, Oklahoma City, OK, U.S.A.

⁴Stoecker & Associates, Rolla, MO, U.S.A.

{re5yb, stanleyj, wvs, jrh55c}@mst.edu, {long, antani}@nlm.nih.gov, gthoma@mail.nih.gov, rosemary-zuna@ouhsc.edu

Keywords: Nuclei Segmentation, Level Set Method, Active Contours, Fuzzy C-means Clustering, Cervical Cancer, Epithelium, Image Processing.

Abstract: Digitized histology images are analyzed by expert pathologists in one of several approaches to assess pre-cervical cancer conditions such as cervical intraepithelial neoplasia (CIN). Many image analysis studies focus on detection of nuclei features to classify the epithelium into the CIN grades. The current study focuses on nuclei segmentation based on level set active contour segmentation and fuzzy c-means clustering methods. Logical operations applied to morphological post-processing operations are used to smooth the image and to remove non-nuclei objects. On a 71-image dataset of digitized histology images (where the ground truth is the epithelial mask which helps in eliminating the non epithelial regions), the algorithm achieved an overall nuclei segmentation accuracy of 96.47%. We propose a simplified fuzzy spatial cost function that may be generally applicable for any n-class clustering problem of spatially distributed objects.

1 INTRODUCTION

The abnormal growth of squamous cells on the surface of the cervix leads to cervical cancer. Study of microscopic slides of cervical tissue allows early detection of cancer. The thickness of the squamous epithelium on the surface of the cervix and the various nuclei features have been examined in previous studies (Krishnan et al., 2012) to determine the grades of cervical intraepithelial neoplasia (CIN), a cervical cancer precondition. CIN grades include Normal, CIN1, CIN2, and CIN3. CIN1 grade corresponds to initial human papilloma virus (HPV) infection; CIN2 and CIN3 show increasing density of nuclei, and increasing spread of the abnormal area across the epithelium. Examples of the CIN grades are shown in Figure 1.

Many algorithms have been implemented for the extraction of nuclei features from cervix epithelial tissue. Convolutional nets and graph partitioning have been explored for the segmentation of the nuclei and the cytoplasm (Song et al., 2015). This

combination has achieved an accuracy of 90.2%. The accuracy of this algorithm is reduced in cases of overlapping of nuclei or cytoplasm. Another combination in this field uses the K-means clustering for initial segmentation and superpixels for the segmentation of cytoplasm and nucleus (Lu et al., 2013). This paper addresses the segmentation problem of the overlapping cervical cells and achieves a comparably good accuracy using k-means and superpixel segmentation methods.

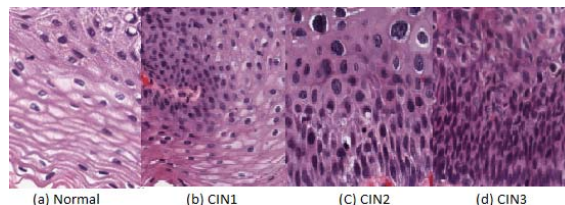


Figure 1: Examples of Four CIN grades.

Other than segmentation, various selected features can also be used for the classification of the images. Fast morphological gray-scale transforms were used

by (Walker et al., 1994) for the image classification. This has utilized GLCM texture features for the identification of traces of cancer, achieving good accuracy and experimental results. Along with these methods, image filtering with K-means clustering for nuclei segmentation along with the other combinational algorithms has been applied in other nuclei studies (Guo et al., 2015) (Rahmadwati et al., 2011). This paper introduces a level set algorithm in combination with fuzzy clustering for the segmentation of the nuclei.

1.1 Fuzzy Clustering and Level Set Algorithm

The level set contour algorithm is combined with an additional algorithm for accurate results. (Wang and Pan, 2014) used the local correntropy-based K-means along with the level set algorithm.

This algorithm helps in eliminating the complex noise present. Similarly, this paper uses spatial fuzzy c-means clustering for the initialization of the level set parameters. These parameters change with respect to the type of input image. Initially, the level set method uses the level set function, which evolves from the zero level set to the boundaries of the object that is being segmented. This function is restricted by the driving force. This force can be either the inverse of the gradient of the image or a Gaussian function which can be a positive constant or a negative force based on the input image. The driving force function is usually the gradient function, because the gradient detects sharp intensity changes in an image. The value of the gradient is high at object edges, indicating a sharp change in intensity. The contour is obtained based on the driving force. A high driving force inside the object allows the contour to expand, while a low driving force at the object edges causes the contour evolution to stop at the object boundaries (Phillips, 1999). In this paper the driving force is controlled by the membership function. The proposed algorithm is shown in the Figure 2. These main steps are explained in the next section.

2 PROPOSED ALGORITHM

2.1 Dataset Description

The images used for the segmentation of the nuclei are from a 71-image dataset. These images are the digitized histology images of hematoxylin and eosin

(H&E) glass slide preparations of uterine cervix biopsy tissue. These images are initially masked to eliminate non-epithelium regions. This masking is done manually. An example input image and associated mask are shown in Figure 3.

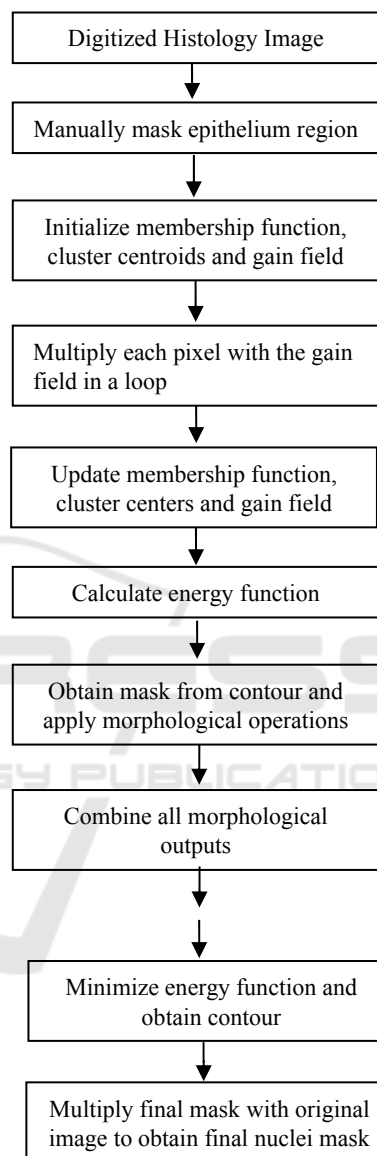


Figure 2: Sequential steps of the proposed algorithm.

2.2 Spatial Fuzzy C-means Clustering

As discussed above spatial information is included in the membership function. The input image is the masked RGB epithelium region from Figure 3 (RGB image is masked with the binary image below) and is used for modeling to include spatial information. A gain field is introduced and is multiplied with

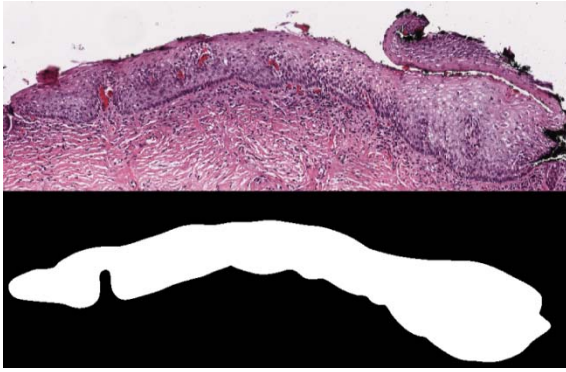


Figure 3: The unmasked (top) and mask of the images of the epithelium.

each and every pixel of the input image. This helps in including the spatial information in each and every pixel rather than using a confined window. The equation for the modeling of the input image is shown below (Balla-Arab et al., 2013).

$$y_i = x_i G_i, \forall i \in \{1, 2, 3, \dots, N\} \quad (1)$$

where y_i and x_i are the observed and the true intensities of the pixel and G_i is the gain field for the i^{th} pixel of the image. N is the total number of pixels present in that image. This modeled image is then used for further analysis in place of the input image. The cost function of this algorithm is modified by introducing the modeled output in place of the general input (Lu, 2013). The general cost function Q and the updated cost function Q' are shown below.

$$Q = \sum_{j=1}^k \sum_{i=1}^N u_{ji}^f \|x_i - v_j\|^2 \quad (2)$$

$$Q' = \sum_{j=1}^k \sum_{i=1}^N u_{ji}^f \|y_i/g_i - v_j\|^2 \quad (3)$$

As we can see, the parameter u indicates the membership function and v_i indicates the centroid of the i^{th} pixel, whereas the parameter ' f ' indicates the amount of fuzziness to be included for each and every cluster. This value is obtained by applying the algorithm on various inputs with various fuzziness values. The final fuzzy value which is used in this algorithm is 2. This parameter controls the amount of fuzziness to be included in the cost function. This helps in introducing the spatial information into the membership function. In general, the minimization of the cost function gives the final clusters and its centers, which are the values obtained after the

convergence. Here the updated cost function is minimized to get the converged cluster centers. We used gradient descent as the minimization method. While minimizing, the first derivatives of the cost function are calculated with respect to the membership function, cluster centers and the gain field. The obtained first derivatives are then equated to zero to get equations which are solved for points that minimize the cost function. These derivatives when set to zero give the final update laws for the membership function, gain field and the cluster centers. The equations for the updated membership function, cluster centers and the gain fields are given below (Balla-Arab et al., 2013).

$$U_k(x, y) = \frac{1}{\sum_{l=1}^a \left(\frac{\|Y(x, y) - B(x, y) - v_k\|}{\|Y(x, y) - B(x, y) - v_l\|} \right)^{\frac{2}{f-1}}} \quad (4)$$

$$v_k(x, y) = \frac{\int_{\omega} U_k^f(x, y) (Y(x, y) - B(x, y)) dx dy}{\int_{\omega} U_k^f(x, y) dx dy} \quad (5)$$

$$B(x, y) = Y(x, y) - \frac{\sum_{j=1}^k U_j^f(x, y) v_j}{\sum_{j=1}^k U_j^f(x, y)} \quad (6)$$

where U_k indicates the membership function of the k^{th} pixel, $Y(x, y)$ is the modeled input image at that particular location. $B(x, y)$ is the bias function which is obtained using the gain field of the modeled image at that location. f indicates the amount of fuzziness to be included in each cluster. \emptyset indicates the whole image whereas ω indicates the part of the image. v_k indicates the centroid of the k^{th} pixel. a indicates the number of clusters.

2.3 Simplified Spatial Cost Membership Function for Optimal Clustering

As we can see, the exponent in the membership function in Equation (4) is $\frac{2}{f-1}$. If the value of f is greater than 2, the membership function increases gradually, which might lead to over clustering; on the other hand, if the value of f is less than 2 and greater than 1, the membership function decreases, and the pixels which are supposed to have high membership function values will have low membership function values, which might lead to under segmentation. To balance these tendencies, we take $f = 2$ as the fuzziness parameter.. (We made this decision based on empirical tests of the algorithm on various input images.) So when f is taken as 2, the membership function reduces to the equation given

by Equation (7).

$$U_k(x, y) = \frac{1}{\sum_{l=1}^a \left(\frac{\|Y(x, y) - B(x, y) - v_k\|}{\|Y(x, y) - B(x, y) - v_l\|} \right)^2} \quad (7)$$

This is the final membership function which is used to derive the energy function of the image and also the driving force which controls the evolution of the level set function. We assume that we need exactly two clusters, one for nuclei and one for non-nuclei. This assumption will give rise to the following equation.

$$U_1(x, y) + U_2(x, y) = 1 \quad (8)$$

2.4 Level Set Active Contour Method

The zero level set in general is from the level set function intersected with a constant plane. This intersection gives a contour in two dimensional space. This is shown in Figure 4, where $\phi(x, y, t)$ is the level set function and $\phi = 0$ is the equation for the zero level set. The red contour obtained is the intersection of the level set function and the plane which is the zero level set. The evolution of the level set function starts from the zero level set and evolves to the edges of the nuclei. In this paper the driving force is obtained from fuzzy c-means clustering by using the fuzzy membership function. The parameters of the level set algorithm which control the evolution are shown in Table 1.

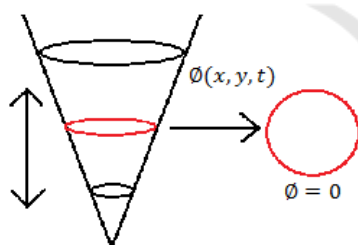


Figure 4: The zero level set is the level set function intersected with a plane.

From Table 1, ‘ τ ’ represents the time step. A larger time step may reduce the evolution time but may result in loss of boundary detail. We used an empirically determined value, after experimentation on various input images. This value varies with the type of input image. ‘ f ’ represents the amount of fuzziness induced by the membership function. We set this value to 2, as discussed above. ‘ $V1$ ’, ‘ $V2$ ’ are the cluster centres, one for the nuclei and one for the non-nuclei regions. ‘ λ ’ is an empirically determined constant which is multiplied by the force function, which was determined as 2.

Table 1: Parameters of level set.

Parameters	Description
τ	Time step of evolution
f	Fuzziness parameter
$V1$	Cluster centre
$V2$	Cluster centre
λ	Multiplicative factor

The equation for the driving force, including the fuzzy membership function, is given below (Ballarab et al., 2013).

$$F = \rho(U_1^f(x, y)\|Y(x, y) - B(x, y) - v_1\|^2 - U_2^f(x, y)\|Y(x, y) - B(x, y) - v_2\|^2) \quad (9)$$

where ρ is a parameter which enhances or reduces the controllability of the driving force. In this paper the value of ρ equals 1. This driving force contains the modeled input image, gain field information, membership function and the cluster centers. These values are obtained from the previously derived equations and are substituted in the equation of the driving force. Minimization of the driving force divides the whole image into the two regions, one for non-nuclei regions and one for nuclei regions. This results in obtaining the contour which stops evolving at the edges of the nuclei. The mask for the epithelium region of the input image is manually marked.

2.5 Morphological Operations

Morphological operations are applied to the output from the level set operation described in section 2.2 to obtain a nuclei mask. Three functions are implemented to clean the mask while retaining the data. These morphological operator outputs help in reducing noise while preserving critical nuclei information from the input. Three functions are applied since the data present in one output may not be present in the other output. Combining all the three outputs gives the best final result. The three functions are demonstrated below.

- i. Small nuclei are retained while removing the large area objects and very small area objects
- ii. Large area nuclei objects are retained while removing the small nuclei objects
- iii. Difference image between i and ii.

The morphological operations are applied to the level set output generated from the masked epithelium region from Figure 3. It is evident that in



Figure 5: Retaining the small nuclei by eliminating large area objects.

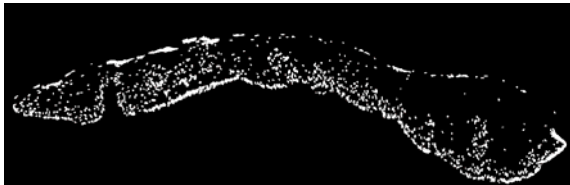


Figure 6: Retaining the large area objects.



Figure 7: Output of the difference.

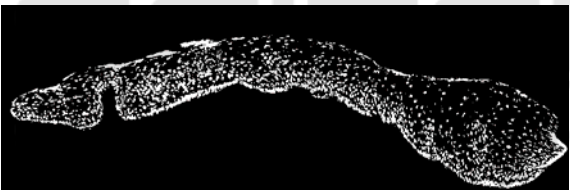


Figure 8: Combined output of the morphological functions.

Figure 5, nuclei with comparatively small size are retained and in Figure 6 nuclei which have large area are retained. Figure 7 is the morphological output of the difference of the previous two images. This helps in retaining the medium sized nuclei present. Figure 8, the final nuclei mask, is the combined output and is free of noise. This nuclei mask when multiplied with the input image, gives the masked nuclei output, shown in Figure 9.

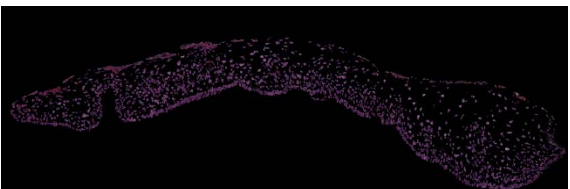


Figure 9: Nuclei Mask.

3 EXPERIMENTS AND RESULTS

This algorithm is applied on various images and the accuracy for all the 71-image dataset is calculated. Examples of false negative and false positive cases are shown below. True positive results are the cases where the detected object is in fact a nucleus, and a false negative result is the case where the nucleus object is not detected; false positive cases and true negative cases indicate non-nuclei objects incorrectly and correctly labeled, respectively.

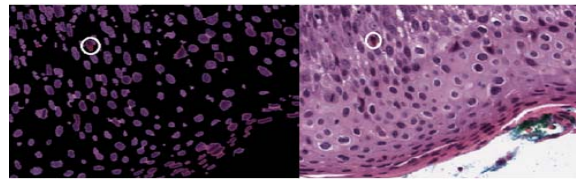


Figure 10: False positive detection example.

As we can see in Figure 10 the circled area in the masked image is not a nucleus but it is detected as nucleus, a false positive.

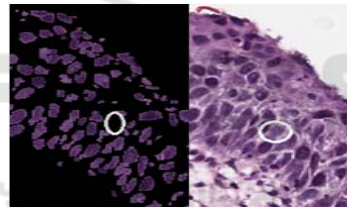


Figure 11: False negative detection example.

In Figure 11 the nucleus shown is not detected and hence this is a false negative result. False negative and false positive cases reduce the overall accuracy. We calculated accuracy based on these visual inspections of the results. The best and the worst cases of the algorithm are shown below.

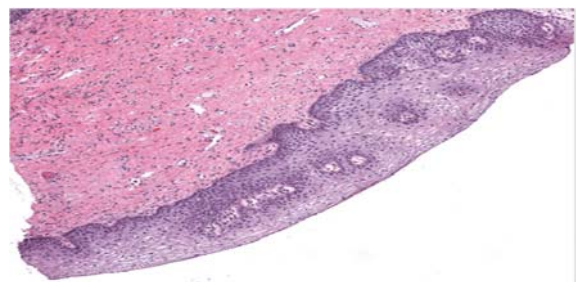


Figure 12: Example of good nuclei segmentation.

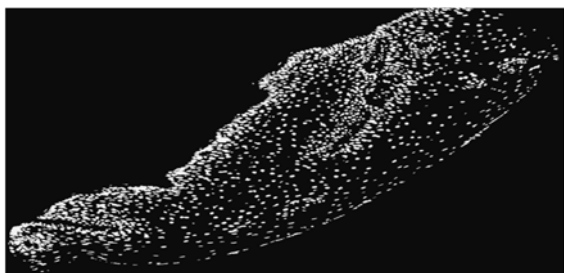


Figure 13: Mask generated.

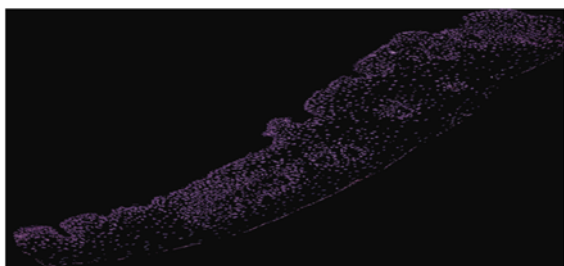


Figure 14: Masked nuclei output.

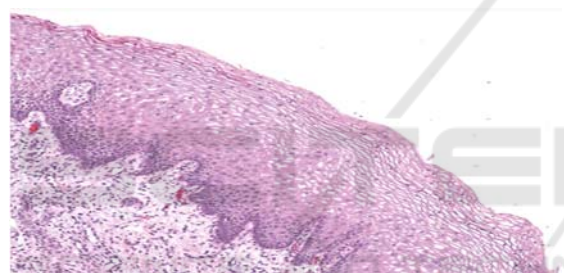


Figure 15: Image example with nuclei detection errors.

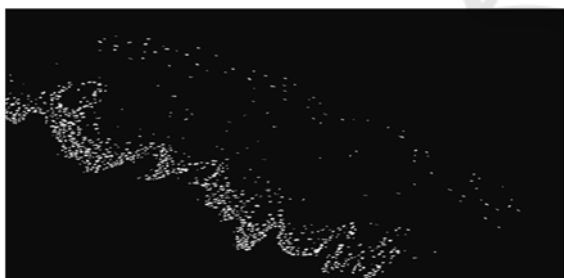


Figure 16: Masked image.



Figure 17: Masked nuclei output.

In most cases the nuclei are detected with good accuracy. For a few input images with smaller nuclei, sensitivity of nuclei detection is less than for the other images. When morphological operations are applied to the binary mask image, smaller sized nuclei get eliminated since they are considered noise. This can be improved by tuning the parameters of the morphological operations.

4 EVALUATION

We calculated nuclei segmentation accuracy by initially calculating the number of nuclei objects detected by the algorithm, and then using human visual inspection to assess true positive, false negative, and false positive. We calculated accuracy from the equation below (Szénási et al., 2012)

$$\text{Accuracy} = \frac{T_p - F_N - F_p}{T_p} \quad (10)$$

where T_p indicates the true positive detections (number of nuclei correctly found), F_N indicates the false negative detections (number of nuclei that are not found) and F_p indicates the false positive detections (number of false nuclei that are found) from the image. For the masked epithelium image from Figure 3 used for demonstration, the nuclei segmentation accuracy obtained is 96.47% ($T_p = 1163, F_N = 4, F_p = 37$). In the experimental results, the accuracy for the best case image is 100% ($T_p = 2164, F_N = 0, F_p = 0$) and the accuracy for the worst case image is 81.98% ($T_p = 827, F_N = 0, F_p = 149$). This accuracy is calculated for each image in the 71-image dataset.

5 COMPARISON

Various investigators have published results on nuclei segmentation. To cite one example (Guo et al., 2015), K-means and other morphological operations have been used and have achieved 88.5% accuracy. This paper segments the initial image into ten vertical segments and then SVM or LDA algorithms are applied and then their results are used for obtaining final classification label. The dataset used is similar and has obtained from NLM database which was discussed earlier. This proposed algorithm presents a nuclei segmentation approach based on the fuzzy c-means and level set segmentation methods and performs the

segmentation of the nuclei on a digitized histology dataset of 71 images. The average accuracy for segmentation results achieved is 96.47%. Table 2 provides a summary of the nuclei detection results for these images

Table 2: Nuclei Segmentation Results, 71-image Dataset.

Total No. Nuclei	T_p	F_p	T_N
75107	73791	1662	346

6 DISCUSSION

The best result, 100% detection of all the nuclei, was achieved for an image where the nuclei were non-overlapping and had larger nuclei as compared to the other test images. A combination of morphology operators is proposed as a method to optimize information preservation while removing noise. In the worst case (81% accuracy), nearly 20% of nuclei were not detected, since many small nuclei were removed in the morphological operations. We experimented with modifying the algorithm to allow small objects to be retained; this increased the accuracy of nuclei detection for one particular image by 10%, at a cost of drop in overall accuracy over the 71-image set of 9%, from 96% to 87%. In our current work, we use the original algorithm and continue to seek an alternate solution which does not degrade the overall accuracy. We propose the simplified spatial cost function Equation (7), as a cost function that may be generally applicable for any N-class clustering problem of spatially distributed objects. Since many problems involve two classes, our novel technique represented in Equation (8) is proposed as an optimal solution to two-class spatial clustering problems.

ACKNOWLEDGEMENTS

This research was supported [in part] by the intramural research program of the National Institutes of Health (NIH), the National Library of Medicine (NLM), and Lister Hill National Center for Biomedical Communications (LHNCBC). We gratefully acknowledge the medical expertise and collaboration of Dr. Mark Schiffman and Dr. Nicolas Wentzensen, both of the National Cancer

Institute's Division of Cancer Epidemiology and Genetics (DCEG).

The relatively small set presented here (71 images) is typical for this domain, with other studies presenting fewer images. The 71 images represent 284 possible grading choices: normal, CIN1, CIN2 and CIN3. The domain addressed here is therefore quite dependent on expert input. The large number of segments, 710, and the large number of nuclei present in each segment, provide a sufficiently large number of nuclei for application of the methods outlined here.

REFERENCES

- Balla-Arab, S., Gao, X. & Wang, B., 2013. A fast and robust level set method for image segmentation using fuzzy clustering and lattice Boltzmann method. *IEEE Transactions on Cybernetics*, 43(3), pp.910–920.
- Guo, P. et al., 2015. Nuclei-Based Features for Uterine Cervical Cancer Histology Image Analysis with Fusion-based Classification. *IEEE journal of biomedical and health informatics*, (c).
- Krishnan, M.M.R. et al., 2012. Computer vision approach to morphometric feature analysis of basal cell nuclei for evaluating malignant potentiality of oral submucous fibrosis. *Journal of Medical Systems*, 36(3), pp.1745–1756.
- Lu, Z., Carneiro, G. & Bradley, A.P., 2013. Automated nucleus and cytoplasm segmentation of overlapping cervical cells. In *Lecture Notes in Computer Science (including subseries Lecture Notes in Artificial Intelligence and Lecture Notes in Bioinformatics)*. pp. 452–460.
- Phillips, C., 1999. The level-set method. *The MIT Undergraduate Journal of Mathematics*, pp.155–164. Available at: [http://diyhl.us/~bryan/papers2/frey/levelsets/Phillips C., The level-set method.pdf](http://diyhl.us/~bryan/papers2/frey/levelsets/Phillips_C.,_The_level-set_method.pdf).
- Rahmadwati, G.N. & Ros, M. & Todd, C. & Norahmawati E., 2011. Cervical cancer classification using Gabor filters. In *First IEEE International Conference on Healthcare Informatics, Imaging and Systems Biology*, pp. 48-52.
- Song, Y. et al., 2015. Accurate segmentation of cervical cytoplasm and nuclei based on multiscale convolutional network and graph partitioning. *IEEE Transactions on Biomedical Engineering*, 62(10), pp.2421–2433.
- Szénási, S., Vámosy, Z. & Kozlovsky, M., 2012. Evaluation and comparison of cell nuclei detection algorithms. In *16th IEEE International Conference on Intelligent Engineering Systems (INES2012)*. pp. 469–475. Available at: http://users.nik.uni-obuda.hu/sanyo/gpgpu/ines2012_submission_101.pdf.
- Walker, R.F. et al., 1994. Classification of cervical cell nuclei using morphological segmentation and textural

feature extraction. In *Intelligent Information Systems, 1994. Proceedings of the 1994 Second Australian and New Zealand Conference on*. pp. 297–301.

Wang, L. & Pan, C., 2014. Robust level set image segmentation via a local correntropy-based K-means clustering. *Pattern Recognition*, 47(5), pp.1917–1925.

